Journal of Genetics and Genomics 53 (2026) 143–153

Contents lists available at ScienceDirect

Journal of Genetics and Genomics

Journal homepage: www.journals.elsevier.com/journal-of-genetics-and-genomics/

Original Research

Two-pore-domain potassium channel Sandman regulates intestinal stem cell homeostasis and tumorigenesis in *Drosophila melanogaster*

Chen Zheng [a, 1], Jiadong Zheng [b, c, d, 1], Xin Wang [e], Yue Zhang [a], Xianjue Ma [b, c, d, *], Li He [a, *]

[a] The First Affiliated Hospital of USTC, Division of Life Sciences and Medicine, University of Science and Technology of China, Hefei, Anhui 230027, China
[b] Key Laboratory of Growth Regulation and Translational Research of Zhejiang Province, School of Life Sciences, Westlake University, Hangzhou, Zhejiang 310024, China
[c] Westlake Laboratory of Life Sciences and Biomedicine, Hangzhou, Zhejiang 310024, China
[d] Institute of Biology, Westlake Institute for Advanced Study, Hangzhou, Zhejiang 310024, China
[e] Department of Oncology, The First Affiliated Hospital of Anhui Medical University, Hefei, Anhui 230022, China

ARTICLE INFO

Article history:
Received 3 March 2025
Received in revised form
8 May 2025
Accepted 9 May 2025
Available online 15 May 2025

Keywords:
Drosophila melanogaster
Potassium channel
Intestinal stem cells
Tumor
ER stress

ABSTRACT

Potassium channels regulate diverse biological processes, ranging from cell proliferation to immune responses. However, the functions of potassium homeostasis and its regulatory mechanisms in adult stem cells and tumors remain poorly characterized. Here, we identify Sandman (Sand), a two-pore-domain potassium channel in *Drosophila melanogaster*, as an essential regulator for the proliferation of intestinal stem cells and malignant tumors, while dispensable for the normal development processes. Mechanistically, loss of *sand* elevates intracellular K^+ concentration, leading to growth inhibition. This phenotype is rescued by pharmacological reduction of intracellular K^+ levels using the K^+ ionophore. Conversely, overexpression of *sand* triggers stem cell death in most regions of the midgut, inhibits tumor growth, and induces a Notch loss-of-function phenotype in the posterior midgut. These effects are mediated predominantly via the induction of endoplasmic reticulum (ER) stress, as demonstrated by the complete rescue of phenotypes through the co-expression of *Ire1* or *Xbp1s*. Additionally, human homologues of Sand demonstrated similar ER stress-inducing capabilities, suggesting an evolutionarily conserved relationship between this channel and ER stress. Together, our findings identify Sand as a shared regulatory node that governs *Drosophila* adult stem cell dynamics and tumorigenesis through bioelectric homeostasis, and reveal a link between the two-pore potassium channel and ER stress signaling.

Introduction

Potassium (K^+) channels, essential for regulating the most abundant cation in the cytosol, play significant roles in multiple biological processes, including the cell cycle, metabolism, cytoskeleton organization, and immune responses (Gonzalez et al., 2012; Xia et al., 2023). Within the potassium channel family, the two-pore domain channels (K_{2P}) represent the newest and least understood members (Natale et al., 2021). Unlike other potassium channel families that function as tetramers, K_{2P} channels operate as homo- or heterodimers (Natale et al., 2021). The human and fly genomes encode 15 K_{2P} and 11 K_{2P} channels, respectively, the functions of most of which remain largely unexplored. K_{2P} channels are generally considered to contribute to background K^+ currents, thus helping maintain the resting membrane potential in excitable cells such as neurons and muscles (Enyedi and Czirjak, 2010). However, recent studies suggest that K_{2P} proteins may play much broader roles across various systems as these proteins are responsive to a wide array of stimuli, including pH changes, anesthetics, antidepressant agents, post-translational modifications, lipids, oxygen tension,

* Corresponding authors.
E-mail addresses: maxianjue@westlake.edu.cn (X. Ma), lihe19@ustc.edu.cn (L. He).
[1] These authors contributed equally to this work.

https://doi.org/10.1016/j.jgg.2025.05.003

temperature, and even mechanical forces (Enyedi and Czirjak, 2010; Natale et al., 2021). This diversity underscores their potential significance in different physiological and pathological conditions.

In *Drosophila melanogaster*, studies on K_{2P} proteins have focused on their roles within the nervous system (Pimentel et al., 2016; Weiss et al., 2019) and heart (Klassen et al., 2017; Abraham et al., 2018), while their functions in non-excitable tissues remain unexplored. In mammals, K_{2P} channels have been linked to tumor development in several studies. The expression of various K_{2P} family proteins is significantly altered in the majority of cancer types (Williams et al., 2013). But only a few K_{2P} channels have been functionally characterized in cancers so far. Specifically, KCNK9 is found to be overexpressed in 35% of lung cancer cases (Mu et al., 2003), and a monoclonal antibody targeting KCNK9 has been shown to inhibit cancer growth and metastasis by inducing its internalization (Sun et al., 2016). Moreover, the loss of KCNK3 has been demonstrated to promote apoptosis and inhibit cell proliferation in lung cancer cells (Wang et al., 2018). However, the precise molecular mechanisms through which K_{2P} channels affect cancer development are not fully understood. It is also unknown whether K_{2P} channels play a role in tumor development in flies. This gap in knowledge underscores the necessity for further research into the roles of K_{2P} channels across different species and tissue types, particularly given the potential implications for understanding and treating cancer.

In the past decade, the *Drosophila* intestinal stem cells (ISCs) have emerged as an important model of adult stem cells and gastrointestinal cancer. This model is particularly appreciated for its conservation of molecular mechanisms with mammals, alongside the advantage of simpler genetic manipulation (Li and Jasper, 2016; Kofman and Levin, 2024). Recent research utilizing this system has identified various ion channels that play roles in maintaining midgut homeostasis, including the Na^+ channel PPK4 (Kim et al., 2017), Cl^- channel CFTR (Kim et al., 2020), and several Ca^{2+} channels such as GluR (Deng et al., 2015), TRPA1 (Xu et al., 2017), PMCA (Deng et al., 2015), and Piezo (He et al., 2018). However, the impact of K^+ homeostasis on ISC proliferation and the channel mediating this regulation in stem cells remains unclear.

In this study, we tackled these knowledge gaps by identifying a K_{2P} channel, *Sandman* (*Sand*), as being essential for the growth of ISCs and malignant tumors. We found that the loss of *Sand* function leads to an accumulation of intracellular K^+, resulting in proliferation inhibition. Additionally, we observed that overexpression of Sand unexpectedly induces significant endoplasmic reticulum (ER) stress and Notch pathway inhibition across various cell types. Finally, we demonstrated that the ability of Sand to induce ER stress is likely to be evolutionarily conserved, as evidenced by specific human *Sand* homologues exhibiting similar ER stress-inducing properties in mammalian cells. These findings offer perspectives on the bioelectric regulation of stem cells and tumors, highlighting K_{2P} channels as a potential therapeutic target for the control of adult stem cells and the treatment of cancer.

Results

Identification of *Sand* as a regulator of intestinal stem cells and malignant tumors

The *Drosophila* genome encodes 11 distinct K_{2P} channels, most of which have been identified in the fly midgut (Buchon et al., 2013; Marianes and Spradling, 2013; Hung et al., 2020) (Fig. S1A and S1B). To investigate the functional impact of K_{2P} knockdown in ISCs, we employed stem cell-specific *esg-Gal4* drivers combined with RNAi lines from the Bloomington *Drosophila* Stock Center. Among the RNAi lines tested, two independent RNAi lines against a K_{2P} protein, Sand, significantly inhibited both self-renewal and the Bleomycin-induced damage repair capabilities of ISCs (Figs. 1A, 1B, S1C, S1D). Knocking down *Sand* using *esg-Gal4* reduced basal stem cell density through all regions of the fly midgut (Figs. 1C, 1D, S2A). Similarly, midgut clones with *Sand* knockdown displayed a significant reduction in clone size, indicative of impaired stem cell proliferation (Fig. S2B and S2C). To further assess whether *Sand* functions cell-autonomously in ISCs, we performed tissue-specific knockdowns using *Gal4* drivers targeting ISCs, enteroblasts (EBs), enterocytes (ECs), and enteroendocrine cells (EEs) (Fig. S2D). Our findings revealed that only the reduction of Sand in ISCs leads to a proliferation phenotype, suggesting that Sand is autonomously required in ISCs. Conversely, overexpression of *Sand* resulted in a unique phenotype within the midgut: while the density of ISCs decreased in most midgut regions (R1−R4), it markedly increased in the posterior R5 region (Figs. 1C, 1D, S2A). Furthermore, Sand overexpression also triggered a strong increase in the number of EEs in the R5 region but not in the R1−R4 regions (Fig. 1D−1H).

Quantitative analysis of the R4 region, serving as a representative for the R1−R4 regions, alongside the R5 region, showed that midgut width decreases in *Sand-RNAi* (*Sand-i*) flies and increases in *Sand*-overexpression (*Sand-OE*) flies. This suggests that the production of enterocytes from stem cells is reduced in *Sand-i* flies but increased in *Sand-OE* flies (Fig. 1E). These observations are supported by changes in the number of GFP^+ cells (driven by *esg-Gal4*) and mitotic cells marked by phospho-Histone 3 (pH3) (Fig. 1F and 1G). Similar alterations were observed in both intestinal precursor cells and EEs within the third instar larval midgut subjected to *Sand-i* and *Sand-OE* (Fig. S3), suggesting that *Sand* regulates ISCs independently of developmental stages. However, a notable discrepancy was the reduction of GFP^+ stem cells specifically in the R1−R4 regions, which may be attributed to either a transient amplification followed by a loss of stem cells or an increased differentiation into enterocytes (Fig. 1F). Furthermore, treatment with Bleomycin exacerbated the growth inhibition observed in *Sand-i* flies without significantly affecting the phenotype of *Sand-OE* flies (Fig. 1I). This treatment also showed the reduction of EEs generation in *Sand-i* (in all midgut regions) and *Sand-OE* (in the R1−R4 regions) (Fig. 1J), revealing a significant difference between the anterior R1−R4 and R5 regions that had not been previously noted.

We further validated the RNAi phenotype with two independent *Sand* knock-out mutants (*Sand-KO*) generated through the CRISPR-Cas9 technique (Bassett and Liu, 2014) (Fig. S4A and S4B). Both *Sand-KO* lines exhibited significant suppression of Bleomycin-induced ISC proliferation in the fly midgut, consistent with the effects observed in *Sand-i* (Fig. 1K and 1L). In contrast, neither *Sand-i* nor *Sand-KO* displayed any notable developmental defects, aligning with previous reports (Pimentel et al., 2016; Abraham et al., 2018; Weiss et al., 2019) (Figs. 1M, 1N, S4C−S4H), suggesting that *Sand* is specifically required in ISCs. However, overexpression of Sand appears to be broadly toxic: ubiquitous expression of Sand using *Tub-Gal4* resulted in complete lethality, while eye-specific expression driven by *ey-Gal4* led to a substantial reduction in organ size (Fig. 1M and 1N).

Previous studies have demonstrated that adult stem cells share similarities with tumors in several aspects, such as self-renewal, epigenetic regulation, telomere maintenance, metabolism, and signaling pathways (Yin et al., 2021). However, it remains unclear whether stem cells and tumors rely on similar molecules for bioelectric regulation. To explore this, we investigated the role of *Sand* in tumor progression within *Drosophila* models. We examined the effects of *Sand* knockdown and overexpression across various classic fly tumor models, including hyperplastic tumors induced by *yki* or Ras^{V12} expression, and invasive neoplastic tumors caused by the combination of Ras^{V12} expression and *lgl* mutation (Wu et al.,

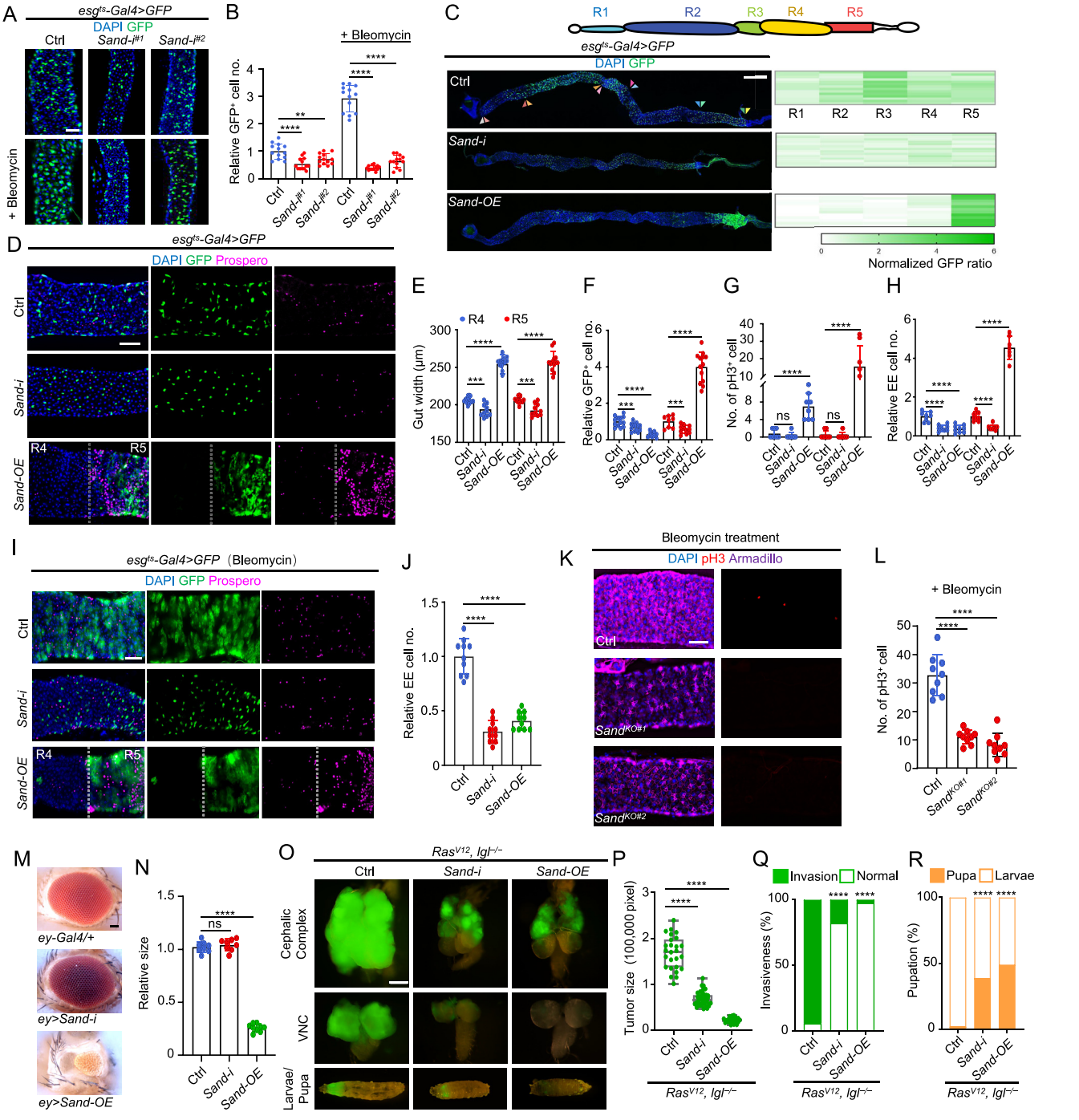

Fig. 1. Identification of *Sand* as a regulator of ISCs proliferation and tumor growth. **A**: Fluorescent micrographs of adult midguts expressing *esg*^{ts}*-Gal4* driver to down-regulate gene expression of *Sand* specifically in GFP-labeled progenitor cells by two individual RNAi lines. Two-to-three-day-old adult females were shifted from 18°C to 29°C for 7 days and then were fed with 5% sucrose or Bleomycin (10 μg/mL in 5% sucrose) for 48 h at 29°C before dissection. Sand was found to result in a reduction of the number of intestinal stem cells. Meanwhile, knockdown of *Sand* significantly reduced stem cell proliferation under Bleomycin treatment. **B**: Quantification of the number of GFP$^+$ cells within 10,000 μm^2 area. The number of counts per group is 13. **C**: The diagram shows the regional pattern of the *Drosophila melanogaster* intestine. The left panel displays fluorescent micrographs of the adult whole gut after 7 days of knockdown and overexpression of *Sand* in ISCs at 29°C. The right panel shows a heatmap of stem cell numbers in regions R1–R5 under the corresponding conditions (n = 14, 14, 12). **D**: Fluorescent micrographs of adult midguts. Knockdown of *Sand* results in a significant reduction of ISCs and EEs. Midguts were immunostained with anti-Prospero antibody to label EEs. Overexpression of *Sand* in regions R4 and R5 exhibited opposite phenotypes: in regions R4, ISCs and EEs significantly decreased; in regions R5, ISCs and EEs significantly increased. **E**: Quantification of the gut width in R4 and R5 (n = 14, 10, 13, 14, 10, 13). **F**: Quantification of the number of GFP$^+$ cells in R4 and R5 regions within 10,000 μm^2 area (n = 13, 13, 9, 8, 11, 13). **G**: Quantification of the number of pH3$^+$ cells in R4 and R5. The number of counts per group is 8. **H**: Quantification of Prospero$^+$ cells in R4 and R5 regions within 10,000 μm^2 area (n = 8, 8, 9, 8, 9, 7). **I** and **J**: Fluorescent micrographs of adult midguts. The numbers of ISCs and EEs did not increase after being fed Bleomycin for 48 h with knockdown and overexpression of *Sand*. For quantification of EEs, n = 10. **K** and **L**: Fluorescent micrographs of adult midguts. After being fed Bleomycin for 48 h, the armadillo staining showed clear cell boundaries and a lower number of pH3$^+$ cells in *Sand* knockout flies, indicating that stem cell proliferation was inhibited. For quantification of pH3$^+$, n = 9. **M** and **N**: Light micrographs of *Drosophila* adult eye side view and quantification of the eye size with indicated genotypes driven by the eye-specific *Gal4*, *ey-Gal4* (n = 8, 8, 9). **O**: Fluorescent micrographs of GFP-labeled Cephalic Complex, VNC, and pupa/larvae are shown with indicated genotypes. Compared with *Ras*^{V12}*;lgl*$^{-/-}$ tumors that induce massive overgrowth, tumors were dramatically suppressed by coexpression of *Sand-i* or *Sand-OE*. **P**–**R**: Quantification of tumor size, invasiveness-related, and pupation-related penetrance observed with indicated genotypes. n = 26, 39, 26 (**P**); n = 36, 39, 40 (**Q**); n = 230, 234, 295 (**R**). All data are presented as mean ± SD. *, $P \leq 0.05$; **, $P < 0.01$; ***, $P < 0.001$; ****,

2008, 2010). Our findings revealed that both knocking down and overexpressing *Sand* significantly suppressed the growth, invasiveness, and lethality associated with Ras^{V12}, $lgl^{-/-}$ tumors in third instar larval Cephalic Complex and ventral nerve cords (VNC) (Fig. 1O−1R). Similarly, *Sand-i* and *Sand-OE* reduced the size of *yki*-induced tumors in these eye discs; however, Ras^{V12}-induced tumors were not significantly affected (Fig. S5). Furthermore, we assessed the impact of *Sand* manipulation on the *yki*- and Ras^{V12}-induced stem cell tumors in the fly midgut. Our results showed that *Sand-i* suppresses both *yki*- and Ras^{V12}-triggered stem cell tumors, whereas *Sand-OE* had minimal effect on either (Fig. S6). These data suggest that fly ISCs and malignant tumors share a common bioelectric regulator, *Sand*, indicating similarities in their regulatory mechanisms.

Nonetheless, distinctions still exist between different cell contexts. The effect of knocking down *Sand* varies across different tumorigenesis conditions, indicating that Sand is required specifically for certain types of tumors. In the fly midgut, Sand is required for both Ras^{V12} and yki overexpression tumors (Fig. S6). However, in fly larval eye-antennal disc tumors, Sand knockdown only affects yki overexpression, and Ras^{V12}, $lgl^{-/-}$ tumors, but not Ras^{V12}-only tumors (Figs. 1O, 1R, S5). The impact of *Sand* overexpression differs among various tumors: *Sand* overexpression fails to inhibit the growth of Ras^{V12} and yki overexpression tumors in fly midgut as well as Ras^{V12} tumor in eye-antennal discs (Figs. S6 and S5), but significantly inhibits the growth of *yki*, and Ras^{V12}, $lgl^{-/-}$ tumors in eye discs (Fig. 1O−1R). It seems that intestinal tumors are more dependent on Sand presence but are more tolerant to Sand overexpression. Conversely, Ras^{V12} tumors in the eye-antennal discs seem insensitive to either a decrease or an increase in Sand levels. This context-dependent requirement underscores the complexity of Sand's role in tumorigenesis and highlights the importance of identifying tissue- and condition-specific factors in determining the effects of Sand in the future.

Loss of *Sand* inhibits stem cell and invasive tumor growth by increasing intracellular potassium

Previous studies in mammalian cells have indicated that blocking K^+ channels can lead to cell cycle arrest, possibly through membrane depolarization (Blackiston et al., 2009). Additionally, a decrease in intracellular K^+ has been associated with the facilitation of cell death (Hughes et al., 1997; Panayiotidis et al., 2006). Based on these findings, we hypothesized that knocking down *Sand* could cause an accumulation of K^+ in intestinal cells, thereby inhibiting cell proliferation. To test this hypothesis, we generated *Sand-i* and *Sand-OE* clones in the fly midgut and stained the dissected midgut with K^+ fluorescent probe, Enhanced Potassium Green-4 AM (EPG-4 AM), which increases green fluorescence after binding of K^+ ions. Our results showed that *Sand-i* cells exhibited a significant increase in EPG-4 signal compared to neighboring control cells, indicating elevated intracellular K^+ levels following the loss of *Sand* (Fig. 2A and 2B). Conversely, overexpression of *Sand* did not significantly alter K^+ concentration.

To further investigate the role of K^+ accumulation in the *Sand* knockdown phenotype, we employed two classic K^+ ionophores, Valinomycin and Nigericin, to manipulate intracellular K^+ levels. Valinomycin, a bacterial polypeptide that forms complexes specifically with K^+ ions, facilitates their transmembrane transport, which also affects the membrane potential (Huang et al., 2021). While Nigericin, a bacterial polyether ionophore, promotes an electroneutral exchange between H^+ and K^+ across the membrane, which does not change membrane potential (Strahl and Hamoen, 2010; Gao et al., 2021). Both Valinomycin and Nigericin treatments reduced the accumulation of intracellular K^+ (Fig. S7). Although these drugs caused a moderate increase in stem cell numbers in control midguts, they significantly rescued the growth inhibition induced by *Sand-i*, restoring it to control levels (Fig. 2C and 2D). In contrast, although Bleomycin and DSS treatment triggered significantly stronger stem cell proliferation in control midguts, they failed to rescue the phenotype in *Sand-i* midguts; while the addition of Valinomycin and Nigericin completely alleviated the inhibition of ISC proliferation caused by *Sand-i* under Bleomycin and DSS treatments (Fig. 2C and 2D). These data suggest that the effect of restoring intracellular K^+ is specific to the *Sand-i*. These observations suggest that the growth inhibition resulting from *Sand* knockdown is likely due to increased K^+ accumulation within the cells rather than changes in membrane potential.

We further evaluated the effects of these drugs on the Ras^{V12}, $lgl^{-/-}$ invasive tumor model in larval Cephalic Complex and VNC. Unfortunately, larvae did not tolerate Nigericin well, resulting in mortality during treatment. In contrast, Valinomycin treatment significantly reversed the growth suppression, reduced invasiveness, and increased pupation rates caused by *Sand-i* (Fig. 2E−2H). Thus, our data strongly suggest that the reduction of *Sand* inhibits ISCs and invasive tumor growth by increasing the cytosolic K^+ concentration.

Overexpression of *Sand* suppresses Notch activity by influencing the trafficking of the Notch receptor

The distinctive phenotypes resulted from *Sand-OE* in the fly midgut have drawn our attention, particularly given the unprecedented regional variations observed. *Sand-OE* not only demonstrated markedly different effects on ISCs between the R1−R4 and R5 regions but also produced seemingly contradictory outcomes: while midgut width and proliferation (as indicated by pH3 staining) increased in R1−R4, the number of ISCs decreased in these regions (Fig. 1C−1H). We hypothesized that this could be due to an initial transient increase in stem cell proliferation followed by a subsequent rise in stem cell loss through either death or differentiation as the phenotype developed. To test this hypothesis, we examined the *Sand-OE* phenotype at various time points (Figs. 3A, 3B, S8A, S8B). Our findings revealed that ISCs hyper-proliferated during the first three days across all midgut regions. However, after five days, stem cell numbers began to decrease in the R1−R4 regions, while cells in the R5 region continued to proliferate excessively. Given the limitations of apoptosis staining in the midgut, we tested whether *Sand-OE* induces cell death using fly wing imaginal discs. Indeed, disc cells overexpressing *Sand* exhibited a significant increase in cleaved-Caspase 3 staining (Fig. 3D), supporting the notion that prolonged expression of *Sand* may lead to increased cell death and subsequent reduction in stem cell numbers. Additionally, the inhibition of cell death by expressing both a dominant-negative form of *Drosophila* caspase ($Dronc^{CARD}$) and baculovirus caspase inhibitor p35 rescued the loss of stem cells caused by *Sand-OE* (Hay et al., 1994; Meier et al., 2000), supporting the notion that apoptosis is the primary cause of stem cell reduction (Fig. S8C and S8D).

In the R5 region of adult midgut, we observed that *Sand-OE* leads to a significant increase in EEs over time (Figs. 1D−1H, 3A−3C). A similar increase in EEs was also observed in the larval midgut (Fig. S3). Additionally, in the R5 region, ISCs marked by *Delta-lacZ* were significantly increased, while EBs, identified by the Notch activity reporter *Su(H)Gbe-lacZ*, were reduced (Fig. S8E−S8H). These observations closely resemble the Notch

$P < 0.0001$; ns, not significant. Ordinary one-way ANOVA followed by Bonferroni's multiple comparisons test was utilized. Scale bars, 50 μm (**M**); 100 μm (**A**, **D**, **I**, **K**); 200 μm (**O**); 400 μm (**C**). no., number; ISCs, intestinal stem cells; EEs, enteroendocrine cells; Ctrl, control; OE, overexpression; DAPI, 4′,6-diamidino-2-phenylindole; VNC, ventral nerve cords; SD, standard deviation.

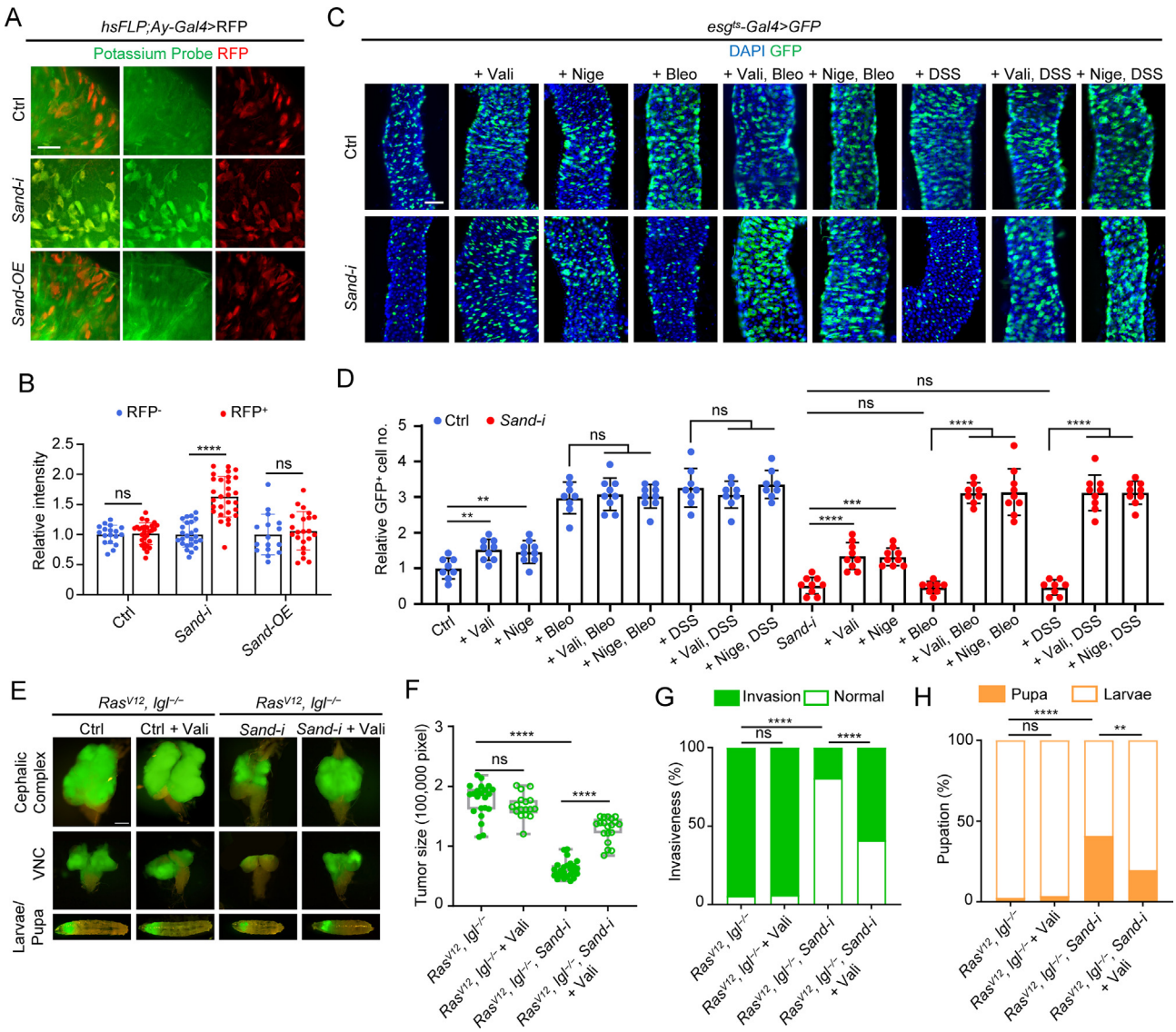

Fig. 2. *Sand* regulated ISCs and tumor growth by increasing cytosolic K^+. **A** and **B**: Fluorescent micrographs of midgut bearing RFP-labeled clones with indicated genotypes stained with potassium ion fluorescent probe, EPG-4 AM to indicate cytosolic K^+ levels. Knockdown of *Sand* leads to an increase in cytosolic K^+ levels, while overexpression of *Sand* does not change the K^+ levels. For quantification of the potassium ion probe fluorescent intensity, $n = 18, 28, 25, 29, 16, 22$. **C** and **D**: Fluorescent micrographs of adult midguts expressing *esg*^{ts}*-Gal4* driver to down-regulate *Sand* expression specifically in GFP-labeled progenitor cells feeding with potassium ionophore-Valinomycin (500 nm/mL in 5% sucrose) and Nigericin (10 μm/mL in 5% sucrose) for 72 h to rescue K^+ levels, while simultaneously administering Bleomycin or DSS. The number of ISCs increased. For quantification of the GFP^+ cells, $n = 8, 9, 9, 8, 9, 9, 8, 8, 8, 9, 9, 9, 8, 8, 9, 8, 9, 9$. **E**: Fluorescent micrographs of GFP-labeled Cephalic Complex, VNCs, and pupa/larvae with indicated genotypes are shown. Compared to the suppression of tumor growth in *Ras*^{V12}*; lgl*$^{-/-}$ with knockdown of *Sand*, feeding valinomycin rescues tumor growth. **F**–**H**: Quantification of tumor size, invasiveness-related and pupation-related penetrance observed with indicated genotypes. $n = 22, 17, 25, 19$ (**F**); $n = 22, 17, 24, 18$ (**G**); $n = 33, 17, 28, 26$ (**H**). All data are presented as mean ± SD. *, $P \leq 0.05$; **, $P < 0.01$; ****, $P < 0.0001$; ns, not significant. Two-tail unpaired Student's *t*-test was utilized in (**A**); Ordinary one-way ANOVA followed by Bonferroni's multiple comparisons test was utilized in (**D**, **F**, **G**, and **H**). Scale bars, 100 μm (**A** and **C**); 200 μm (**E**). ISCs, intestinal stem cells; Ctrl, control; no., number; EPG-4 AM, Enhanced Potassium Green-4 AM; Vali, valinomycin; Nige, nigericin; Bleo, bleomycin; DSS, dextran sodium sulfate; DAPI, 4′,6-diamidino-2-phenylindole; VNC, ventral nerve cords; SD, standard deviation.

loss-of-function phenotype, which promotes stem cell proliferation and EE differentiation but inhibits EB production. To test whether *Sand-OE* inhibits Notch activity in general, we overexpressed *Sand* in third instar larval imaginal disc using *hh-Gal4*. The results showed that *Sand-OE* strongly suppressed the expression of the Notch downstream gene *Cut* and the Notch activity reporter *NRE-lacZ* (Figs. 3E and S9A). In addition, overexpressing *Sand* in the adult wing by *hh-Gal4* showed a missing wing margin (Fig. 3F). Overexpression of *Sand* in the thorax by *pnr-Gal4* showed a multi-bristle phenotype (Fig. S9B). Both phenotypes are classic signs of Notch inhibition.

To investigate the mechanism by which *Sand-OE* affects Notch signaling, we performed staining of the Notch receptor using an antibody against the Notch intracellular domain (NICD). Our results showed a significant accumulation of intracellular Notch receptor in *Sand-OE* wing imaginal discs (Fig. 3G and 3H). This effect on the Notch receptor is not limited to the wing disc epithelium; *Sand-OE* clones generated in the third instar fat body also exhibited increased intracellular Notch receptor staining (Fig. 3I and 3J). Conversely, the level of Notch ligand Delta was not affected (Fig. S9C). Previous studies have shown that the Notch receptor undergoes proteinase cleavage and post-translational modification in the ER, disruptions to which can lead to intracellular accumulation of the receptor and subsequent signaling inactivation (Hounjet and Vooijs, 2021). Our data suggest that *Sand-OE* inhibits Notch activation, likely by interfering with the trafficking of the Notch receptor.

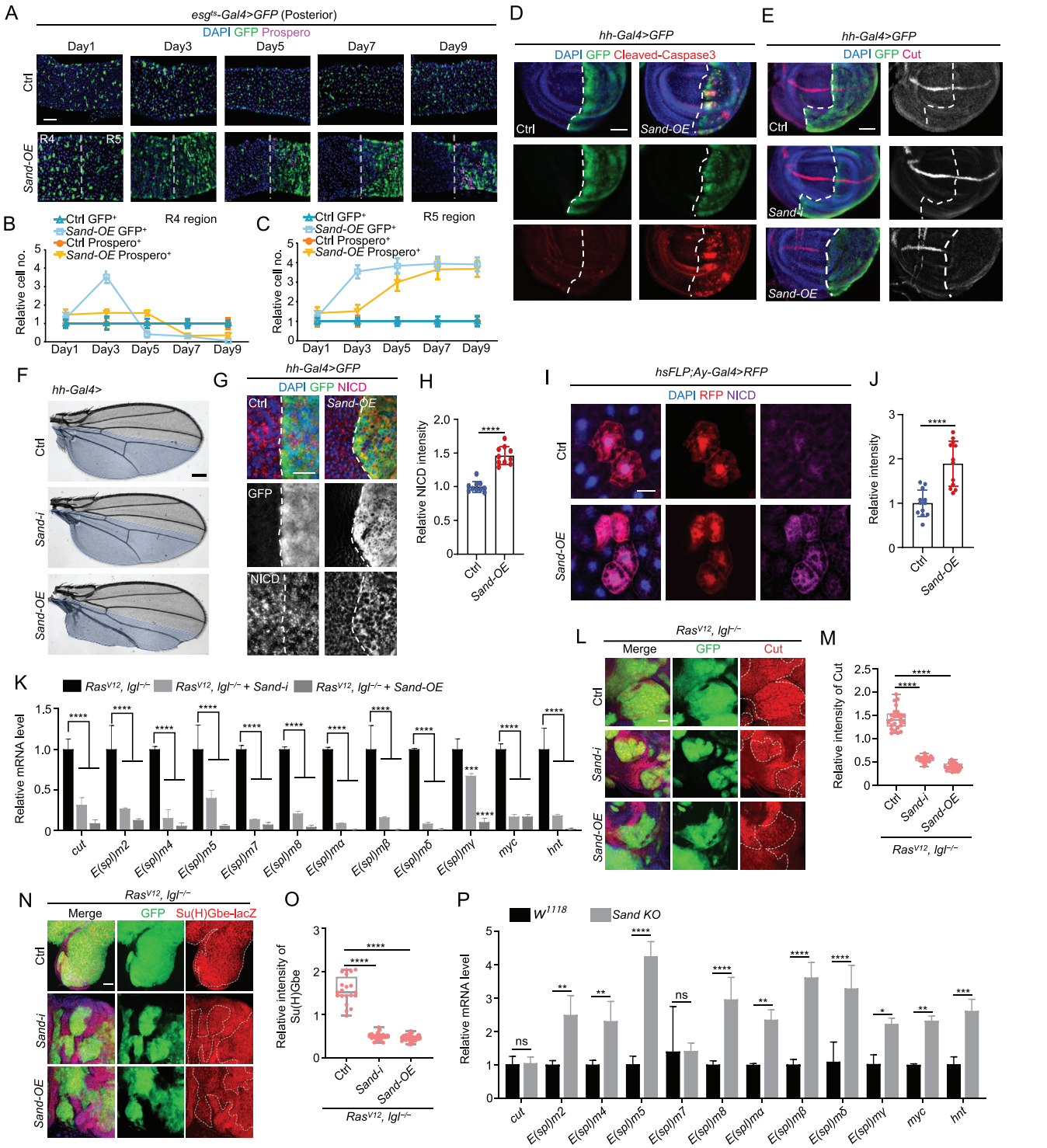

Fig. 3. *Sand* overexpression inhibits Notch activity in multiple tissues. **A**: Fluorescent micrographs of adult midguts expressing *esg*^{ts}*-Gal4* driver to overexpression of *Sand* at different time points specifically in GFP-labeled progenitor cells. With varying durations of overexpression, the number of ISCs and EEs decreased in region R4, while they increased in region R5. **B** and **C**: Quantification of the change in ISCs and EEs numbers over time in regions R4 (**B**) and R5 (**C**). The number of counts per group is 10. **D**: Fluorescent micrographs of wing discs immunostained with anti-cleaved Caspase3 to label the apoptosis level. Cells are labeled by GFP expression along the A/P boundary (dashed lines) under control of the *hh-Gal4* driver. **E**: Fluorescent micrographs of wing discs immunostained with anti−Cut antibody to label Cut transcription. Cells are labeled by GFP expression along the A/P boundary (dashed lines) under control of the *hh-Gal4* driver. **F**: Images of adult wings showing the posterior half (indicated by blue shading) expressing the indicated genes driven by *hh-Gal4*. **G** and **H**: Fluorescent micrographs of wing discs immunostained with anti-NICD antibody to label Notch transcription. Cells are labeled by GFP expression along the A/P boundary (dashed lines) under control of the *hh-Gal4* driver. For quantification of the relative intensity of NICD, $n = 10$. **I** and **J**: Fluorescent micrographs of fat body bearing RFP-labeled clones with indicated genotypes immunostained with anti-NICD antibody to indicate NICD transcription. For quantification of the relative intensity of NICD, $n = 12$. **K**: Quantification of the relative fold change of target gene expression in the Notch pathway with indicated genotypes. *Rp49* mRNA was used as an internal control. **L** and **N**: Eye discs bearing GFP-labeled clones with indicated genotypes were immunostained with anti-Cut (**L**) or anti-lacZ (**N**) antibody. **M** and **O**: Quantification of the relative intensity of Cut (**M**) and Su(H)Gbe (**O**) with indicated genotypes. $n = 25$, 21, 31 (**M**); $n = 20$, 26, 41 (**O**). **P**: Quantification of the relative fold change of target gene expression in the Notch pathway with indicated genotypes in the gut. *Rp49* mRNA was used as an internal control. All data are presented as mean ± SD; **, $P < 0.01$; ***, $P < 0.001$; ****, $P < 0.0001$; ns, not significant. Two-tailed unpaired Student's *t*-test was utilized in (**H**, **J**, **K**,

Additionally, to determine whether the *Sand-OE* phenotype is caused by hyperpolarization of the cell membrane, we overexpressed *Kir2.1*, a classic inward-rectifier potassium channel commonly used to hyperpolarize neurons (Hodge, 2009), and examined if its overexpression would trigger similar phenotypes like *Sand-OE*. Our results showed that overexpression of *Kir2.1* did not significantly affect stem cell density (Fig. S9D and S9E), suggesting that the phenotypes observed with *Sand-OE* are likely caused by mechanisms other than membrane potential increase.

We further examined the effects of *Sand-OE* and *Sand-i* on various Notch target genes in the Ras^{V12}, $lgl^{-/-}$ tumors. Again, all the tested Notch downstream genes were sufficiently reduced in the *Sand-OE* samples compared to controls (Fig. 3K). Staining of Notch target gene *Cut* and Notch activity reporter *Su(H)Gbe-lacZ* also showed strong reduction of Notch activity in the *Sand-OE* tumors relative to control tumors (Fig. 3L−3O). This reduction was also evident in wild-type disc epithelium and *yki*-induced tumors (Fig. S10). However, *Sand-i* also markedly reduced Notch target genes in the Ras^{V12}, $lgl^{-/-}$ tumors (Fig. 3L−3O), suggesting a complex mechanism between *Sand* levels and Notch regulation in malignant tumors. To test the effect of *Sand* knockdown in normal tissue, we examined the Notch target genes in the wild-type and *Sand-KO* midguts. Knocking out *Sand* significantly increases the mRNAs of most Notch target genes in the midgut, showing that *Sand* consistently inhibited Notch signaling in intestinal tissues (Fig. 3P). Collectively, these data suggest that while *Sand* suppressed the Notch signaling across multiple tissues, including adult and larval midguts, imaginal discs, and specific tumor types, this regulatory relationship remains context-dependent.

The *Sand* overexpression phenotype is primarily mediated by an increase in ER stress

The progressive development of the *Sand-OE* phenotype in the R1−R4 regions of the midgut suggests that *Sand* overexpression may induce certain chronic cellular stress in ISCs. Initially, this stress triggers a compensatory proliferation response in ISCs, similar to the effects of many other cell-damaging agents (Markstein et al., 2014). However, prolonged stress eventually leads to increased cell death, which outweighs the initial proliferative effect and reduces the number of stem cells in the R1−R4 regions. Meanwhile, the inhibition of Notch receptor trafficking makes us suspect that *Sand* overexpression may trigger ER stress, which blocks proper processing of the Notch receptor. Increased ER stress has previously been shown to trigger ISC proliferation in the fly midgut (Wang et al., 2014). While sustained and unmitigated ER stress has been found to trigger cell death (Szalai et al., 2018), which can explain the loss of ISCs after prolonged expression of *Sand*. Moreover, a recent study in mammalian intestinal organoids reported that increased ER stress triggers ISC to EE differentiation (Sittipo et al., 2021), a phenotype also consistent with our observations of *Sand-OE*.

To test this hypothesis, we manipulated various components of the ER stress machinery to either enhance or reduce ER stress signaling alongside *Sand-OE*. Our experiments showed that mutants reducing the ER's capacity to mitigate ER stress significantly exacerbated the *Sand-OE* phenotype and led to a more pronounced stem cell loss (Fig. 4A and 4B). Specifically, knocking down the major ER-located chaperon *Bip* or expressing a dominant-negative *Bip* mutant (Bip K97S), which impairs the ER's ability to manage ER stress (Pobre et al., 2019), resulted in significant cell death in the R5 region. Additionally, knocking down *Ire1* or *Xbp1*, which mediate the primary downstream responses of ER stress (Fu and Doroudgar, 2022), also caused similar cell death phenotypes in the R5 region. Notably, manipulation of the ER stress machinery alone did not drastically affect ISC number, indicating that *Sand-OE* functions synergistically with the ER stress pathway.

In contrast to the exacerbation of the *Sand-OE* phenotype by reducing ER stress mitigation, expressing downstream effectors of the ER stress effectors, *Ire1* or activated *Xbp1s* (*Xbp1*), completely rescued the *Sand* overexpression phenotype (Fig. 4A and 4B). Previous studies have demonstrated that enhancing the expression of Ire1 can lead to its auto-activation (Martinez-Turtos et al., 2022). Activation of the Ire1−Xbp1s pathway significantly boosts the ER's protein folding and degradation capacities (Fu and Doroudgar, 2022). These findings strongly support the hypothesis that the *Sand* overexpression phenotype is likely caused by ER stress. Moreover, we observed that expressing *Sand* in *Drosophila* S2 cells resulted in a strong accumulation of Sand within the ER (Fig. 4C), supporting a potential function of Sand in ER homeostasis.

To further investigate the role of Sand in ER stress, we utilized the flip-out system to generate *Sand* overexpression clones in the fat body of third instar larvae. Our result showed that *Sand-OE* triggered a strong UPR, as indicated by the phosphorylation of eIF2α, a marker for ER stress. Importantly, this effect was fully rescued by co-expression of *Ire1* or *Xbp1s* (Fig. 4D and 4E). Similarly, the abnormal accumulation of the Notch receptor observed in *Sand-OE* clones was also rescued by co-expression of *Ire1* or *Xbp1s* (Fig. 4F and 4G). This provides additional support for the hypothesis that the aberrant accumulation of the Notch receptor is a consequence of ER stress. Previous studies have demonstrated that ER stress is often accompanied by significant leakage of Ca^{2+} from the ER into the cytosol. As increased ER-to-cytosol Ca^{2+} efflux has been shown to exacerbate ER stress and can even lead to cell death (Lindner et al., 2020). Consistently, we observed a significant increase in cytosolic Ca^{2+} activity in ISCs with *Sand-OE* (Fig. 4H and 4I). To further explore the relationship between ER Ca^{2+} levels and the *Sand-OE* phenotype, we reduced ER Ca^{2+} concentrations using two approaches: expressing Gαq, which triggers ER Ca^{2+} release via activation of the PLC-IP_3-DAG signaling, or knocking down the ER Ca^{2+} pump SERCA, which decreases the transport of Ca^{2+} from the cytosol back into the ER (Carreras-Sureda et al., 2018). Both methods led to strong cell death in region R5 (Fig. S11A and S11B), supporting the conclusion that the *Sand-OE* phenotype is driven by ER stress. Additionally, the *Xbp1>dsRed* transcriptional reporter is significantly activated by *Sand* overexpression in the midgut (Ryoo et al., 2013) (Fig. S11C). Importantly, the *Xbp1>dsRed* activity is much lower in the R5 region compared to the other regions, suggesting that the R5 region tends to maintain an inherently low level of ER stress. This may explain why stem cells are not lost in the R5 region of *Sand-OE* midguts. However, the mechanism responsible for this reduced ER stress in the R5 region remains to be investigated in future studies. We then tested whether the physiological level of Sand contributes to the ER stress level in the fly midgut by testing the expression level of the major ER stress target genes. Compared to wild-type, midgut from *Sand* KO flies showed a significant reduction of ER stress target genes, suggesting that Sand regulates ER stress under physiological conditions (Fig. 4J).

Finally, we wonder if this gain-of-function *Sand* phenotype is conserved in mammals. Humans contain 15 different K_{2P} channels that all share similar homologues with *Sand* (Fig. S12A). To find whether certain mammalian K_{2P} protein induce ER stress similarly to

and **P**); Ordinary one-way ANOVA followed by Bonferroni's multiple comparisons test was utilized in (**M** and **O**). Scale bars, 100 μm (**A**); 50 μm (**D**, **E**, **G**, **H**, **L**); 200 μm (**K**); 30 μm (**L**). ISCs, intestinal stem cells; Ctrl, control; OE, overexpression; no., number; A/P, anterior/posterior; NICD, Notch intracellular domain; KO, knockout; DAPI, 4′,6-diamidino-2-phenylindole; SD, standard deviation.

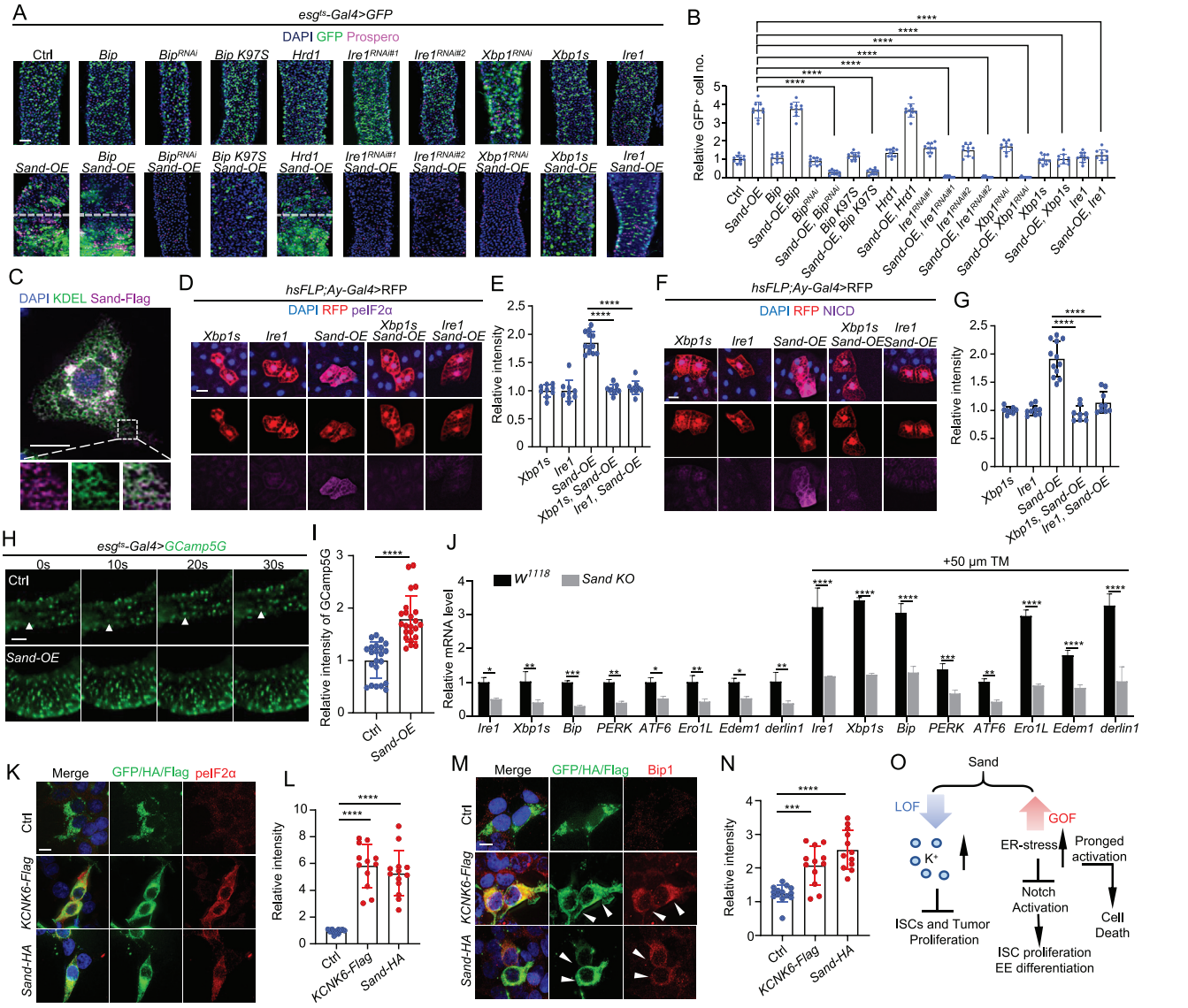

Fig. 4. *Sand* increases triggers ER stress that causes Notch inhibition. **A** and **B**: Fluorescent micrographs of adult midguts expressing *esg*^{ts}*-Gal4* driver to activate/down-regulate the expression of ER stress-related genes with overexpression of *Sand* specifically in GFP-labeled progenitor cells. Quantification of the number of GFP^{+} cells. The number of counts per group is 10. **C**: Fluorescent micrographs of S2 cells immunostained with anti-KDEL and anti-Flag antibody to indicate ER and Sand-Flag subcellular location. **D** and **E**: Fluorescent micrographs of fat body bearing RFP-labeled clones with anti-peIF2α antibody. For quantification of the relative intensity of peIF2α, $n = 9, 9, 12, 9, 9$. **F** and **G**: Fluorescent micrographs of RFP-labeled clones with anti-NICD antibody. For quantification of the relative intensity of NICD, $n = 8, 9, 12, 8, 9$. **H** and **I**: Fluorescent micrographs of adult midguts expressing *esg*^{ts}*-Gal4* driver to coexpress *GCaMP5G* and *Sand*. Overexpression of *Sand* in stem cells results in a constant high Ca^{2+} level rather than an oscillating Ca^{2+} in the control. For quantification of the intensity of GCaMP5G, $n = 22$ and 23. **J**: Quantification of the relative fold change of ER stress-related genes in *Sand* KO gut without and with 50 μm TM treatment for 24 h. *Rp49* mRNA was used as an internal control. **K** and **M**: Fluorescent micrographs of transfection of KCNK6 and Sand induced increased ER stress in HEK293T. **L**: For quantification of the relative intensity of peIF2α, $n = 11, 12, 13$. **N**: For quantification of the relative intensity of Bip1, $n = 14, 12, 12$. **O**: Schema diagram of the functional mechanisms of Sand alternations. All data are presented as mean ± SD; ****, $P < 0.0001$; ns, not significant. Two-tail unpaired Student's *t*-test was utilized in (**I** and **K**); Ordinary one-way ANOVA followed by Bonferroni's multiple comparisons test was utilized in (**B**, **E**, **G**). Scale bars, 100 μm (**A** and **H**); 5 μm (**C**, **K**, **M**); 30 μm (**D** and **F**). Ctrl, control; OE, overexpression; no., number; ER, endoplasmic reticulum; KO, knockout; TM, tunicamycin; ISCs, intestinal stem cells; DAPI, 4′,6-diamidino-2-phenylindole; SD, standard deviation.

fly Sand, we first examined the subcellular localization of different K_{2P} channels in mammalian cells (Fig. S12B). Interestingly, we found several channels, including KCNK3, KCNK6, KCNK10, KCNK13, and KCNK17, showing clear ER location. Further staining of ER stress marker Xbp1s showed that overexpression of KCNK6 and KCNK17 significantly induced ER stress (Fig. S13A and S13B). Using the TCGA database, we found that KCNK6 expression is highly correlated with almost all ER stress genes in all tumors (Fig. S13C and S13D), suggesting KCNK6 is likely to contribute to a higher level of ER stress in different types of cancers. We also investigated whether Sand overexpression could trigger ER stress in mammalian cells. Our experiments demonstrated that cells overexpressing either fly Sand or human KCNK6 exhibited a significant increase in the mRNA level of most ER stress markers, as well as protein levels in phosphorylated eIF2α, Bip, and nuclear accumulation of Xbp1s (Figs. 4K–4N, S14). These observations suggest that the contribution to ER homeostasis by K_{2P} channels is probably evolutionarily conserved.

Discussion

Previous studies on two-pore potassium channels and various types of potassium channels have predominantly focused on their roles in excitable cells such as neurons and myocytes, while research on their functions in non-excitable cells remains relatively limited.

This study identified and preliminarily characterized the biological functions of the K_{2P} protein Sand in ISCs and aggressive tumors. A conventional view posits that K^+ channels influence cell proliferation by modulating membrane potential to regulate cell cycle progression (Delisi et al., 2024). However, our findings in *Drosophila* ISCs suggest that intracellular potassium ion concentration elevation may play a more crucial role. This is supported by pharmacological experiments demonstrating that nigericin feeding in *Drosophila* effectively rescued the *Sand* knockdown phenotype through potassium concentration modulation rather than membrane potential alteration (Strahl and Hamoen, 2010; Gao et al., 2021) (Fig. 2C and 2D). These results indicate that potassium homeostasis imbalance may constitute the core mechanism through which *Sand* regulates cell proliferation, consistent with previous observations linking elevated potassium levels to cell cycle arrest (Urrego et al., 2014).

We found that the gain-of-function of *Sand* significantly induced ER stress and inhibited growth in multiple *Drosophila* tissues (except the R5 region of the midgut), providing a perspective for understanding the complex relationship between K_{2P} channels and tumor progression. And we also discovered that, similar to Sand, the human KCNK6 and KCNK17 channels also trigger significant ER stress when overexpressed in mammalian cells. Similar to our findings, mild ER stress have been found to increases proliferation of mammalian pancreatic β-cells and *Drosophila* intestinal stem cells (Sharma et al., 2015; Wang et al., 2015), while prolonged strong ER stress can eventually trigger cell death (Fu et al., 2021).

Moreover, K_{2P} channels exhibit upregulation or downregulation in various tumor types with distinct prognostic impacts (Williams et al., 2013). For instance, KCNK9 expression is elevated in breast cancer (Mu et al., 2003), colorectal cancer (Kim et al., 2004), and melanoma tissues (Pocsai et al., 2006). Increased KCNK2 expression in prostate adenocarcinoma promotes tumor proliferation, as evidenced by suppressed cancer cell growth upon KCNK2 knockdown (Voloshyna et al., 2008). Conversely, KCNK17 serves as a favorable prognostic marker in lung cancer, suggesting its tumor-suppressive potential (Li et al., 2019). KCNK1 also displays context-dependent roles, with elevated expression correlating with poor prognosis in pancreatic and renal cancers but favorable outcomes in hepatocellular carcinoma. These findings collectively highlight the intricate regulatory roles of K_{2P} proteins in tumor progression. Our study suggests that moderate K_{2P} expression promotes cell proliferation, whereas insufficient or excessive K_{2P} levels lead to cytosolic potassium accumulation or ER stress-mediated suppression of proliferation, respectively. These observations raise critical questions about whether the positive correlation between K_{2P} channel expression and patient survival in specific cancers stems from their tumor-suppressive mechanisms via enhanced ER stress. Furthermore, our findings suggest two distinct therapeutic strategies for tumors with elevated K_{2P} expression: 1) employing potassium channel inhibitors to induce ionic imbalance, and 2) utilizing ER stress-inducing agents to synergize with high K_{2P} levels for apoptosis induction.

Notably, *Sand* overexpression induced markedly different proliferation-differentiation patterns in *Drosophila* midgut R5-region ISCs compared to other regions, potentially indicating unique cellular properties across intestinal compartments. Spatial transcriptomic analysis and clonal studies have previously identified R1−R5 partitioning in the *Drosophila* midgut, where ISCs generate progeny restricted to their native regions (Marianes and Spradling, 2013), though the molecular basis for these regional differences remains unclear. High-fat diets have been shown to induce ER stress (Chen et al., 2016) and impair ISC stemness (Sittipo et al., 2021). Feeding *Drosophila* cholesterol-enriched diets inhibits Notch receptor trafficking, suppresses Notch signaling activation, and promotes enteroendocrine cell differentiation in a region-specific manner, predominantly in the posterior midgut (Obniski et al., 2018)—a phenotype strikingly similar to *Sand* overexpression effects. These parallel findings suggest regional heterogeneity in ER stress responses along the intestinal tract, likely reflecting divergent molecular mechanisms of stress adaptation in distinct gut regions. The underlying mechanisms driving such compartmentalized responses warrant further investigation, potentially revealing insights into regional stem cell characteristics and the maintenance of intestinal domain boundaries.

Further investigations revealed that *Sand* overexpression significantly suppresses Notch signaling, a pathway frequently hyperactivated in colorectal cancer and other malignancies, where it promotes tumor proliferation, invasion, metastasis, therapy resistance, and poor prognosis (Brisset et al., 2023). Notably, *Sand* overexpression shares mechanistic similarities with thapsigargin: both induce apoptosis through ER calcium depletion, ER stress, and Notch signaling inhibition (Lindner et al., 2020; Jaskulska et al., 2020). Importantly, *Sand* overexpression synergizes with other ER stress activators to amplify apoptotic responses, suggesting that tumors with upregulated K_{2P} channels may exhibit heightened sensitivity to ER stress-targeting drugs like thapsigargin. This finding provides a theoretical foundation for optimizing combination therapies in precision oncology.

Finally, the molecular mechanisms underlying Sand-mediated regulation of ISC proliferation and differentiation still require further exploration. While this study established that Sand inhibits Notch receptor trafficking and activation via ER stress induction, the precise regulatory details remain incompletely understood. Previous in vitro studies demonstrated that ER calcium loss blocks Notch signaling by impairing receptor transport (Roti et al., 2013; Pagliaro et al., 2021), a phenomenon corroborated in vivo during ISC differentiation (He et al., 2018; Baghdadi et al., 2024). A defining feature of K_{2P} channels is their functional dimeric structure. Relevant studies in COS-7 cells revealed that KCNK6 overexpression causes ER retention and functional impairment unless co-expressed with an unidentified subunit required for plasma membrane localization (Salinas et al., 1999). Current data cannot definitively determine whether Sand-induced ER stress primarily results from disrupted ER ionic homeostasis or channel-independent functions. The absence of loss-of-function mutants for *Drosophila* K_{2P} channels currently limits this analysis. Future work may employ protein interaction profiling, comparative sequence analysis, and targeted mutagenesis approaches to comprehensively elucidate the molecular mechanisms underlying the cellular functions of *Sand*.

Materials and methods

Fly husbandry and fly stocks

Stocks and crosses were maintained at 25°C or 29°C on standard cornmeal food (3000 mL water, 20 g agar, 120 g yeast, 168 g cornmeal, 264 g glucose, 3.75 g methylparaben, 30 mL propionic acid, total 3 L of fly food) with 12 h:12 h light:dark cycles. For transgene expression using the Gal4/Gal80ts system, crosses were kept at 18°C, two-to-three-day-old adult females were shifted from 18°C to 29°C to induce UAS transgene expression for 7 days before dissection. Wild-type or mutant clones were generated in eye-antennal discs using the mosaic analysis with a repressible marker (MARCM) with ey-Flp. Exact genotypes used for each experiment can be found in Table S1.

Molecular cloning and generation of transgenic flies

The *UAS-Sand* was generated by insertion of the *Sand* into a fly pVALIUM10-roe vector through Gateway recombination. To generate

Sand knockout lines, the initial transcription of *Sand* was cloned into the pDonor vector by 1000 bp each. Three gRNA were designed according to the sequence of the initial transcription location and cloned into the PCFD3 vector. The UAS-*Sand* transgenic flies were generated by injecting embryos using PhiC31-mediated site-specific recombination. The KO flies were generated by injecting embryos of BDSC#78782. Embryo injection was done by UniHuaii Corporation.

Immunofluorescence and imaging

Adult midgut or larval midguts, imaginal discs, Cephalic Complex, and ventral nerve cords were carefully dissected in cold PBS and promptly fixed with 4% paraformaldehyde for a period of 30 min at room temperature. The samples were subjected to continuous shaking during this process and were subsequently washed three times with PBS containing 0.1% Triton X-100 (PBST). To prevent non-specific binding, the samples were blocked in PBS supplemented with 2% Bovine Serum Albumin (BSA) for 1 h at room temperature. They were then incubated overnight at 4°C with primary antibodies specific to the target proteins. Following thorough washing with PBST, the samples were incubated with secondary antibodies for 2 h at room temperature. After additional washes with PBST, the samples were mounted using a DAPI-containing mounting medium and imaged using a Leica DFC9000 sCMOS confocal microscope (inverted) equipped with 20× and 63× oil objectives, allowing for detailed visualization and analysis.

Drug treatment

Two-to-three-day-old adult females with specified genotypes were carefully transferred from a temperature of 18°C−29°C to initiate UAS transgene expression, which was allowed to proceed for 7 days. Subsequently, these adult females were deprived of food in empty vials for a period of 2 h before being offered a 5% sucrose solution, either with or without the addition of 10 μg/mL Bleomycin, 5% DSS, 500 nm/mL Valinomycin, 10 μm/mL Nigericin, 50 μm tunicamycin. This solution was placed on filter paper.

Ex vivo GCaMP imaging in midgut

The midgut was carefully dissected and immersed in complete Schneider's medium (obtained from Sigma, and fortified with 10% FBS as well as 1% streptomycin and penicillin). Utilizing a transfer pipet, the dissected gut was gently placed at the center of a 35-mm dish featuring a 20-mm glass bottom (Nest, 801001), accompanied by a droplet of Schneider's medium, approximately 20 μL in volume. Following this, a 1 cm^2 cellulose tea-bag paper was positioned atop the fat body to facilitate its spreading. Subsequently, a stainless-steel ring with a diameter of 1 cm was delicately placed over the film to prevent the tissue from floating. Finally, 200 μL of the complete Schneider's medium was added to the gut. The Ca^{2+} activity, as reported by GCaMP5G, was closely monitored for a minimum duration of 5 min. All the imaging investigations were conducted employing a Leica M205 FCA high-resolution stereo fluorescence microscopy.

RNA isolation and RT-qPCR

Total RNAs were isolated from adult tissue utilizing an RNA preparation kit, and reverse transcription was conducted in accordance with the manufacturer's protocols. Quantitative PCR was subsequently performed employing the SYBR Green Realtime PCR Master Mix. The relative abundance of mRNA was determined using the ΔΔCt method, with *GAPDH* or *Rp49* mRNA serving as internal controls. Primer can be found in Table S2.

Statistical analysis

The statistical analyses were conducted using GraphPad Prism version 8.0 software. Unless otherwise specified, statistical significance was determined through unpaired, two-tailed Student's *t*-tests. For comparisons involving three or more groups, an ordinary ANOVA test was employed, followed by Bonferroni's multiple comparisons test. In cases where a Gaussian distribution was not assumed, the Mann-Whitney *U* test was applied. The log-rank test was performed for the Kaplan-Meier analysis. A *P*-value of less than 0.05 was considered statistically significant. Data are presented as the mean ± standard deviation (SD). The following notations indicate significance levels: ns, not significant; *, $P \leq 0.05$; **, $P < 0.01$; ***, $P < 0.001$; ****, $P < 0.0001$. All experiments were performed with $n \geq 3$ independent replicates. The number of flies analyzed is indicated in the legend of each figure.

Data availability

All data generated or analyzed in this study are included in the main text or the Supplementary materials. The raw data generated in this study are provided in the Source Data file in this paper. Exact genotypes used for each experiment are listed in Table S1. RT-qPCR primers are listed in Table S2. Reagents and resources are provided in Table S3.

CRediT authorship contribution statement

Chen Zheng: Data curation, Formal analysis, Investigation, Methodology, Visualization, Writing - Original draft, Writing - Review & Editing. **Jiadong Zheng**: Data curation, Formal analysis, Writing - Original draft. **Xin Wang**: Data curation, Formal analysis, Investigation. **Yue Zhang**: Data curation, Formal analysis. **Xianjue Ma**: Conceptualization, Funding acquisition, Supervision. **Li He**: Conceptualization, Funding acquisition, Project administration, Supervision, Writing - Review & Editing.

Conflict of interest

The authors declare no conflict of interest.

Acknowledgments

This project was supported by the National Natural Science Foundation of China to L.H. (32470754 and 32070750) and to X.M. (32170824 and 32322027), and HRHI program of Westlake Laboratory of Life Sciences and Biomedicine to X.M. (1011103360222B1).

Supplementary data

Supplementary data to this article can be found online at https://doi.org/10.1016/j.jgg.2025.05.003.

References

Abraham, D.M., Lee, T.E., Watson, L.J., Mao, L., Chandok, G., Wang, H.G., Frangakis, S., Pitt, G.S., Shah, S.H., Wolf, M.J., et al., 2018. The two-pore domain potassium channel TREK-1 mediates cardiac fibrosis and diastolic dysfunction. J. Clin. Investig. 128, 4843−4855.

Baghdadi, M.B., Houtekamer, R.M., Perrin, L., Rao-Bhatia, A., Whelen, M., Decker, L., Bergert, M., Perez-Gonzalez, C., Bouras, R., Gropplero, G., et al., 2024. PIEZO-dependent mechanosensing is essential for intestinal stem cell fate decision and maintenance. Science 386, eadj7615.

Bassett, A.R., Liu, J.L., 2014. CRISPR/Cas9 and genome editing in *Drosophila*. J. Genet. Genom. 41, 7−19.

Blackiston, D.J., McLaughlin, K.A., Levin, M., 2009. Bioelectric controls of cell proliferation: ion channels, membrane voltage and the cell cycle. Cell Cycle 8, 3527−3536.

Brisset, M., Mehlen, P., Meurette, O., Hollande, F., 2023. Notch receptor/ligand diversity: contribution to colorectal cancer stem cell heterogeneity. Front. Cell Dev. Biol. 11, 1231416.
Buchon, N., Osman, D., David, F.P., Fang, H.Y., Boquete, J.P., Deplancke, B., Lemaitre, B., 2013. Morphological and molecular characterization of adult midgut compartmentalization in *Drosophila*. Cell Rep. 3, 1725–1738.
Carreras-Sureda, A., Pihan, P., Hetz, C., 2018. Calcium signaling at the endoplasmic reticulum: fine-tuning stress responses. Cell Calcium 70, 24–31.
Chen, Y., Wu, Z., Zhao, S., Xiang, R., 2016. Chemical chaperones reduce ER stress and adipose tissue inflammation in high fat diet-induced mouse model of obesity. Sci. Rep. 6, 27486.
Delisi, D., Eskandari, N., Gentile, S., 2024. Membrane potential: a new hallmark of cancer. Adv. Cancer Res. 164, 93–110.
Deng, H., Gerencser, A.A., Jasper, H., 2015. Signal integration by Ca^{2+} regulates intestinal stem-cell activity. Nature 528, 212–217.
Enyedi, P., Czirjak, G., 2010. Molecular background of leak K^+ currents: two-pore domain potassium channels. Physiol. Rev. 90, 559–605.
Fu, F., Doroudgar, S., 2022. IRE1/XBP1 and endoplasmic reticulum signaling - from basic to translational research for cardiovascular disease. Curr. Opin. Physiol. 28, 100552.
Fu, X., Cui, J., Meng, X., Jiang, P., Zheng, Q., Zhao, W., Chen, X., 2021. Endoplasmic reticulum stress, cell death and tumor: association between endoplasmic reticulum stress and the apoptosis pathway in tumors. Oncol. Rep. 45, 801–808.
Gao, G., Liu, F., Xu, Z., Wan, D., Han, Y., Kuang, Y., Wang, Q., Zhi, Q., 2021. Evidence of nigericin as a potential therapeutic candidate for cancers: a review. Biomed. Pharmacother. 137, 111262.
Gonzalez, C., Baez-Nieto, D., Valencia, I., Oyarzun, I., Rojas, P., Naranjo, D., Latorre, R., 2012. K^+ channels: function-structural overview. Compr. Physiol. 2, 2087–2149.
Hay, B.A., Wolff, T., Rubin, G.M., 1994. Expression of baculovirus P35 prevents cell death in *Drosophila*. Development 120, 2121–2129.
He, L., Si, G., Huang, J., Samuel, A.D.T., Perrimon, N., 2018. Mechanical regulation of stem-cell differentiation by the stretch-activated Piezo channel. Nature 555, 103–106.
Hodge, J.J., 2009. Ion channels to inactivate neurons in *Drosophila*. Front. Mol. Neurosci. 2, 13.
Hounjet, J., Vooijs, M., 2021. The role of intracellular trafficking of notch receptors in ligand-independent notch activation. Biomolecules 11, 1369.
Huang, S., Liu, Y., Liu, W.Q., Neubauer, P., Li, J., 2021. The nonribosomal peptide valinomycin: from discovery to bioactivity and biosynthesis. Microorganisms 9, 780.
Hughes Jr., F.M., Bortner, C.D., Purdy, G.D., Cidlowski, J.A., 1997. Intracellular K^+ suppresses the activation of apoptosis in lymphocytes. J. Biol. Chem. 272, 30567–30576.
Hung, R.J., Hu, Y., Kirchner, R., Liu, Y., Xu, C., Comjean, A., Tattikota, S.G., Li, F., Song, W., Ho Sui, S., et al., 2020. A cell atlas of the adult *Drosophila* midgut. Proc. Natl. Acad. Sci. U. S. A. 117, 1514–1523.
Jaskulska, A., Janecka, A.E., Gach-Janczak, K., 2020. Thapsigargin-from traditional medicine to anticancer drug. Int. J. Mol. Sci. 22, 4.
Kim, C.J., Cho, Y.G., Jeong, S.W., Kim, Y.S., Kim, S.Y., Nam, S.W., Lee, S.H., Yoo, N.J., Lee, J.Y., Park, W.S., 2004. Altered expression of KCNK9 in colorectal cancers. APMIS 112, 588–594.
Kim, K., Hung, R.J., Perrimon, N., 2017. miR-263a regulates ENaC to maintain osmotic and intestinal stem cell homeostasis in *Drosophila*. Dev. Cell 40, 23–36.
Kim, K., Lane, E.A., Saftien, A., Wang, H., Xu, Y., Wirtz-Peitz, F., Perrimon, N., 2020. *Drosophila* as a model for studying cystic fibrosis pathophysiology of the gastrointestinal system. Proc. Natl. Acad. Sci. U. S. A. 117, 10357–10367.
Klassen, M.P., Peters, C.J., Zhou, S., Williams, H.H., Jan, L.Y., Jan, Y.N., 2017. Age-dependent diastolic heart failure in an in vivo *Drosophila* model. Elife 6, e20851.
Kofman, K., Levin, M., 2024. Bioelectric pharmacology of cancer: a systematic review of ion channel drugs affecting the cancer phenotype. Prog. Biophys. Mol. Biol. 191, 25–39.
Li, H., Jasper, H., 2016. Gastrointestinal stem cells in health and disease: from flies to humans. Dis. Model. Mech. 9, 487–499.
Li, W.C., Xiong, Z.Y., Huang, P.Z., Liao, Y.J., Li, Q.X., Yao, Z.C., Liao, Y.D., Xu, S.L., Zhou, H., Wang, Q.L., et al., 2019. KCNK levels are prognostic and diagnostic markers for hepatocellular carcinoma. Aging (Albany NY) 11, 8169–8182.
Lindner, P., Christensen, S.B., Nissen, P., Moller, J.V., Engedal, N., 2020. Cell death induced by the ER stressor thapsigargin involves death receptor 5, a non-autophagic function of MAP1LC3B, and distinct contributions from unfolded protein response components. Cell Commun. Signal. 18, 12.
Marianes, A., Spradling, A.C., 2013. Physiological and stem cell compartmentalization within the *Drosophila* midgut. Elife 2, e00886.
Markstein, M., Dettorre, S., Cho, J., Neumuller, R.A., Craig-Muller, S., Perrimon, N., 2014. Systematic screen of chemotherapeutics in *Drosophila* stem cell tumors. Proc. Natl. Acad. Sci. U. S. A. 111, 4530–4535.
Martinez-Turtos, A., Paul, R., Grima-Reyes, M., Issaoui, H., Krug, A., Mhaidly, R., Bossowski, J.P., Chiche, J., Marchetti, S., Verhoeyen, E., et al., 2022. IRE1α overexpression in malignant cells limits tumor progression by inducing an anti-cancer immune response. OncoImmunology 11, 2116844.
Meier, P., Silke, J., Leevers, S.J., Evan, G.I., 2000. The *Drosophila* caspase DRONC is regulated by DIAP1. EMBO J. 19, 598–611.
Mu, D., Chen, L., Zhang, X., See, L.H., Koch, C.M., Yen, C., Tong, J.J., Spiegel, L., Nguyen, K.C., Servoss, A., et al., 2003. Genomic amplification and oncogenic properties of the *KCNK9* potassium channel gene. Cancer Cell 3, 297–302.
Natale, A.M., Deal, P.E., Minor Jr., D.L., 2021. Structural insights into the mechanisms and pharmacology of K_{2P} potassium channels. J. Mol. Biol. 433, 166995.
Obniski, R., Sieber, M., Spradling, A.C., 2018. Dietary lipids modulate notch signaling and influence adult intestinal development and metabolism in *Drosophila*. Dev. Cell 47, 98–111.
Pagliaro, L., Marchesini, M., Roti, G., 2021. Targeting oncogenic notch signaling with SERCA inhibitors. J. Hematol. Oncol. 14, 8.
Panayiotidis, M.I., Bortner, C.D., Cidlowski, J.A., 2006. On the mechanism of ionic regulation of apoptosis: would the Na^+/K^+-ATPase please stand up? Acta. Physiologist 187, 205–215.
Pimentel, D., Donlea, J.M., Talbot, C.B., Song, S.M., Thurston, A.J.F., Miesenbock, G., 2016. Operation of a homeostatic sleep switch. Nature 536, 333–337.
Pobre, K.F.R., Poet, G.J., Hendershot, L.M., 2019. The endoplasmic reticulum (ER) chaperone BiP is a master regulator of ER functions: getting by with a little help from ERdj friends. J. Biol. Chem. 294, 2098–2108.
Pocsai, K., Kosztka, L., Bakondi, G., Gonczi, M., Fodor, J., Dienes, B., Szentesi, P., Kovacs, I., Feniger-Barish, R., Kopf, E., et al., 2006. Melanoma cells exhibit strong intracellular TASK-3-specific immunopositivity in both tissue sections and cell culture. Cell. Mol. Life Sci. 63, 2364–2376.
Roti, G., Carlton, A., Ross, K.N., Markstein, M., Pajcini, K., Su, A.H., Perrimon, N., Pear, W.S., Kung, A.L., Blacklow, S.C., et al., 2013. Complementary genomic screens identify SERCA as a therapeutic target in NOTCH1 mutated cancer. Cancer Cell 23, 390–405.
Ryoo, H.D., Li, J., Kang, M.J., 2013. *Drosophila* XBP1 expression reporter marks cells under endoplasmic reticulum stress and with high protein secretory load. PLoS ONE 8, e75774.
Salinas, M., Reyes, R., Lesage, F., Fosset, M., Heurteaux, C., Romey, G., Lazdunski, M., 1999. Cloning of a new mouse two-P domain channel subunit and a human homologue with a unique pore structure. J. Biol. Chem. 274, 11751–11760.
Sharma, R.B., O'Donnell, A.C., Stamateris, R.E., Ha, B., McCloskey, K.M., Reynolds, P.R., Arvan, P., Alonso, L.C., 2015. Insulin demand regulates beta cell number via the unfolded protein response. J. Clin. Investig. 125, 3831–3846.
Sittipo, P., Kim, H.K., Han, J., Lee, M.R., Lee, Y.K., 2021. Vitamin D_3 suppresses intestinal epithelial stemness via ER stress induction in intestinal organoids. Stem Cell Res. Ther. 12, 285.
Strahl, H., Hamoen, L.W., 2010. Membrane potential is important for bacterial cell division. Proc. Natl. Acad. Sci. U. S. A. 107, 12281–12286.
Sun, H., Luo, L., Lal, B., Ma, X., Chen, L., Hann, C.L., Fulton, A.M., Leahy, D.J., Laterra, J., Li, M., 2016. A monoclonal antibody against KCNK9 K^+channel extracellular domain inhibits tumour growth and metastasis. Nat. Commun. 7, 10339.
Szalai, P., Parys, J.B., Bultynck, G., Christensen, S.B., Nissen, P., Moller, J.V., Engedal, N., 2018. Nonlinear relationship between ER Ca^{2+} depletion versus induction of the unfolded protein response, autophagy inhibition, and cell death. Cell Calcium 76, 48–61.
Urrego, D., Tomczak, A.P., Zahed, F., Stuhmer, W., Pardo, L.A., 2014. Potassium channels in cell cycle and cell proliferation. Philos. Trans. R. Soc. Lond. B Biol. Sci. 369, 20130094.
Voloshyna, I., Besana, A., Castillo, M., Matos, T., Weinstein, I.B., Mansukhani, M., Robinson, R.B., Cordon-Cardo, C., Feinmark, S.J., 2008. TREK-1 is a novel molecular target in prostate cancer. Cancer Res. 68, 1197–1203.
Wang, L., Zeng, X., Ryoo, H.D., Jasper, H., 2014. Integration of UPRER and oxidative stress signaling in the control of intestinal stem cell proliferation. PLoS Genet. 10, e1004568.
Wang, L., Ryoo, H.D., Qi, Y., Jasper, H., 2015. PERK limits *Drosophila* lifespan by promoting intestinal stem cell proliferation in response to ER stress. PLoS Genet. 11, e1005220.
Wang, X.G., Yuan, N.X., Li, X.P., Chen, F.F., 2018. TASK-1 induces gefitinib resistance by promoting cancer initiating cell formation and epithelial-mesenchymal transition in lung cancer. Exp. Ther. Med. 15, 365–370.
Weiss, S., Melom, J.E., Ormerod, K.G., Zhang, Y.V., Littleton, J.T., 2019. Glial Ca^{2+} signaling links endocytosis to K^+ buffering around neuronal somas to regulate excitability. Elife 8, e44186.
Williams, S., Bateman, A., O'Kelly, I., 2013. Altered expression of two-pore domain potassium (K_{2P}) channels in cancer. PLoS ONE 8, e74589.
Wu, M., Pastor-Pareja, J.C., Xu, T., 2010. Interaction between Ras^{V12} and scribbled clones induces tumour growth and invasion. Nature 463, 545–548.
Wu, S., Liu, Y., Zheng, Y., Dong, J., Pan, D., 2008. The TEAD/TEF family protein scalloped mediates transcriptional output of the Hippo growth-regulatory pathway. Dev. Cell 14, 388–398.
Xia, C., Liu, C., Ren, S., Cai, Y., Zhang, Q., Xia, C., 2023. Potassium channels, tumorigenesis and targeted drugs. Biomed. Pharmacother. 162, 114673.
Xu, C., Luo, J., He, L., Montell, C., Perrimon, N., 2017. Oxidative stress induces stem cell proliferation via TRPA1/RyR-mediated Ca^{2+} signaling in the *Drosophila* midgut. Elife 6, e22441.
Yin, W., Wang, J., Jiang, L., James Kang, Y., 2021. Cancer and stem cells. Exp. Biol. Med. 246, 1791–1801.